 doi:10.20944/preprints202210.0438.v1

Article

Investigation of Dynamic Analysis of Corrosion Effect under to Chloride Induced in Reinforced Concrete Bridge Columns

Abdolreza Tangtakabi[1], Mohammad Hasan Ramesht[2*], Ali Golsoorat Pahlaviani[2] and Towhid Pourostam[2]

[1] Department of Civil Engineering, Islamic Azad University, Central Tehran Branch, Iran
[2] Department of Civil Engineering, Islamic Azad University, Central Tehran Branch, Iran
*Corresponding author: mhramesht@yahoo.com

Abstract: One of the influential factors in estimating the service life of reinforced concrete bridges (RCB) is determining the long-term seismic performance of these structures. Corrosion due to chloride ion diffusion leads to the destruction of critical members of the RCB during the useful life of the structure. So, the long-term seismic performance of the bridge deteriorates as a result. It is essential to study the effect of corrosion deterioration on the long-term seismic performance of bridges in the southern regions of Iran, near the coasts of the Persian Gulf and the Oman Sea, because of the seismicity of the region and high corrosion rate of reinforced concrete (RC) members is the result of environmental conditions. In order to investigate this issue, considering studies about environmental conditions of southern Iran, the onset time of corrosion in the columns, as seismic critical members of the bridge, was determined. Based on that, the corrosion's effect on characteristics of RC at specific time points during the bridge's useful life (0, 15, 30, 45, 60, 75 and 90 years) have been calculated. The effects of corrosion include deterioration of the core and cover concrete properties, steel bar and the connection between concrete and steel bar. In the next step, at each time point, according to the modified stress-strain relationships, the moment-curvature analysis of the bridge pier was done, and the properties of the plastic hinge were determined. Finally, based on the obtained data about plastic hinge characteristics at each time point, overload analysis of the bridge was performed in both longitudinal and transverse directions. Then the capacity curves of RCB were compared at the mentioned time-points. The results show that the capacity of the bridge deteriorates over time due to corrosion. Therefore, a proposal to increase the value of base shear design has been made to ensure the long-term seismic performance of RCB in corrosive environments.

Keywords: reinforced concrete bridge (RCB); chloride corrosion; seismic performance; plastic hinge; overload analysis

1. Introduction

The prevailing demolition mechanism for concrete bridges in marine environments with high humidity and salt concentration is corrosion due to chloride ions diffusion. Corrosion significantly reduces the bearing capacity and ductility of RC structures in chloride-rich environments [1, 2]. During the service life of the structure, a gradual decrease in the performance of these structures is due to cracking, destruction of cover concrete [3], reduction of core concrete strength [4], cross-section reduction of steel rebar and deterioration of its mechanical characteristics [5, 6] as well as reduction of connection between concrete and steel bar [7, 8]. The long-term performance of bridges and their service life is a significant issue for maintenance, improvement and repair of such structures. One of the effective factors in estimating the service life of RCB in seismic areas is determining the long-term seismic performance of these structures. Corrosion due to chloride ion diffusion leads to the destruction of critical members of the RCB during the useful life of the structure and thus degrades the long-term seismic performance of the bridge. Therefore, it can be concluded that the RCB that has been designed based on seismic requirements of a specific regulation cannot have the same safety margin as the critical members of the

 doi:10.20944/preprints202210.0438.v1

bridge that suffer significant corrosion. Methods for evaluating the seismic performance of RCB in corrosive conditions during their useful life are important to ensure the safety of the structure and provide an appropriate strategy for structure maintenance. Some studies have been done recently regarding this subject. In most of these studies, the seismic performance of RCB, subjected to corrosion damages, were investigated using the concepts of brittleness curve, structure reliability and finally cost estimation of the structure. The time-dependent reliability of RCB with different structural systems exposed to long-term invasive chloride environments has been investigated in various studies [9 and 10]. Decreased reliability of structures is due to the long-term effect of corrosion. Based on corrosion-induced decay, a kind of probabilistic evaluation method has been proposed to estimate the service life and maintenance strategies of structures under corrosion [11]. Various approaches have been proposed to investigate the general effects of corrosion on the RC members' properties as well as this issue on the structural system's response and their design [14-12]. A study was done to investigate the combined effect of the cumulative damage caused by multiple earthquakes and corrosion-induced decay during the useful life of RCB on the seismic fragility curve of the bridge [15]. The fragility cure determines the probability of the bridge's failure in a given seismic intensity measurement at a given time. Numerous studies have been conducted on the development of the seismic fragility curve of RCB subjected to corrosion [18-16]. Studies show that increasing the probability of failure in certain seismic intensities is proportional to the increase in time and level of corrosion occurred in the structure. From another perspective, general approaches for various types of nonlinear analysis of concrete bridges under corrosion are presented [19, 20]. The southern regions of Iran near the shores of the Persian Gulf and the Oman Sea are one of the most corrosive environments in the world due to high temperature and humidity, strong winds, high-temperature fluctuations and high chloride concentration [21]. Due to high intensity of corrosion of RC members caused by environmental conditions as well as seismicity of the region, it will be important to investigate the effect of corrosion deterioration on long-term seismic performance of bridges in these areas. In this study, the effect of chloride corrosion on the long-term seismic performance of RCB in this area has been investigated using nonlinear (overload) static analysis. First, the onset time of corrosion in the RC columns of the bridge is estimated. Then the possible effects of corrosion, including decay of core and cover concrete properties, longitudinal and transverse steel and the connection between concrete and steel at specific time-points on the useful life of the bridge are calculated. In the next step, based on the material model developed in the previous section, the moment-curvature analysis of the columns was performed at selected time points and based on them, the behavioral characteristics of the columns' plastic hinge were determined. Finally, the bridge's overload analysis in both longitudinal and transverse directions has been done in these time-points, and the capacity curves of the bridge have been developed. Comparison of the obtained capacity curves shows the reduction of bridge capacity in both longitudinal and transverse directions over time due to the effect of corrosion. By comparing the obtained values, a proposal to increase the base shear value is given in order to ensure the long-term seismic performance of the RCB in corrosive environmental conditions. Under aggressive marine environment, the offshore reinforced concrete structures are vulnerable to the attack of various harmful ions like sulfate ions, chloride ions and magnesium ions [22]. In addition, the chloride-induced reinforcement corrosion can also significantly influence the durability of concrete structures [23, 24]. Chloride ions normally exist in pore solution in the form of free ions or be bound by the hydrated product which could slow down the ingress of chlorides [25-27].

Preprints (www.preprints.org) | NOT PEER-REVIEWED | "Posted: 28 October 2022" doi:10.20944/preprints202210.0438.v1

2. Effects of Corrosion on Properties of the Materials

This section describes how to model all possible effects of corrosion (due to the chloride ions penetration) on the mechanical properties of the materials. These effects include the deterioration of the unconfined concrete (cover) and confined concrete (core) properties, longitudinal and transverse steel bar and the connection between concrete and steel.

2.1. Corrosion onset Time and Corrosion Level

The deterioration of the structures related to the corrosion process of steel bar consists of three phases: the first phase as the diffusion phase in which chloride ions are dispersed on the surface of the steel bar, the second phase as the developing phase from the onset of corrosion to when cover concrete starts cracking. The third phase is the decay phase which is the phase after the onset of cracking. In order to simulate the theory and mathematics of the mentioned phases, several models of chloride ion corrosion have been proposed based on Fick's second law. According to the developed models, the concentration of concrete chloride is a function of depth and time on a one-dimensional solution of Fick's second law [1].

$$C(x,t) = C_s\left[1 - \text{erf}\left(\frac{x}{2\sqrt{D_s \times t}}\right)\right] \quad (1)$$

Where:
C(x, t): Concrete chloride concentration
C_s: Chloride concentration at the surface
D_s: Apparent chloride diffusion coefficient
X: Depth from the concrete surface
t: Time
erf (): Error function

Steel bar corrosion begins once the chloride concentration at the bar surface reaches the critical chloride concentration. Based on the existing environmental conditions, different functions have been introduced for the critical chloride concentration and corrosion onset time. Considering that this study is about the RCB in southern Iran, adjacent to the Persian Gulf, the proposed function has been used for this specific region. In this study, the onset time of corrosion is proposed as a result of laboratory studies (simulated environmental conditions of the Persian Gulf and Oman Sea) as well as experimental studies in real corrosive environmental conditions of the southern regions [28]:

$$T_{Corr} = 0.75\left(\frac{d_c}{B_1}\right)^{C_1} \quad (2)$$

Where:
T_{Corr}: Onset time of corrosion (year)
d_c: Thickness of steel bar coat (mm)
B_1 and C_1: Fixed coefficients

Coefficients B_1 and C_1 depend on the water-cement ratio and the percentage of microsilica used in the concrete mixture design. The diameter of the steel bar in RC decreases over time due to corrosion. Based on the calculated corrosion onset time, the following equation is proposed to calculate the reduced diameter of the corrosion-induced steel bar [29]:

$$d_b = d_{bi} - \frac{1.0508(1 - w/c)^{-1.64}}{d_c}(t - T_{Corr})^{0.71} \quad (3)$$

Where:
d_b: Reduced steel bar diameter
d_{bi}: Initial diameter of steel bar

 doi:10.20944/preprints202210.0438.v1

w/c: water-cement ratio

Based on the reduced diameter of the steel bar due to corrosion, the amount of corrosion (Δ_{Corr}) is defined as follows:

$$\Delta_{Corr} = \frac{d_b^2 - d_{bi}^2}{d_{bi}^2} \times 100 \quad (4)$$

First, corrosion occurs in the bar, and then, due to the expansion of the corrosion products, cracking occurs in the cover and core concrete.

2.2. Effect of Corrosion on Unconfined Concrete (Cover) Properties

The volumetric expansion of corrosion products of steel reinforcement causes perimeter tensile stress and development of tensile strain in concrete and ultimately leads to cracking and rupture of cover concrete. The created perimeter tensile strain is calculated as follows [20]:

$$\varepsilon_r = \frac{\sum w_{cr}}{b_0} \quad (5)$$

Where:

ε_r: Transverse tensile strain

Σw_{cr}: Crack width of the entire longitudinal and transverse bar (mm)

b_0: Concrete cross-section circumference (mm)

The corresponding crack width for steel bars is determined using the following equation:

$$w_{cr} = \pi(\nu_{rs} - 1)(2x) \quad (6)$$

Where:

2x: Reduced diameter of the steel bar due to corrosion

ν_{rs}: Expansion coefficient of steel bar diameter due to corrosion

The value of ν_{rs} coefficient in this study is considered to be 2. The width of the crack created by the corrosion of the longitudinal and transverse bars is shown in Fig. 1.

Preprints (www.preprints.org) | NOT PEER-REVIEWED | "Posted: 28 October 2022" doi:10.20944/preprints202210.0438.v1

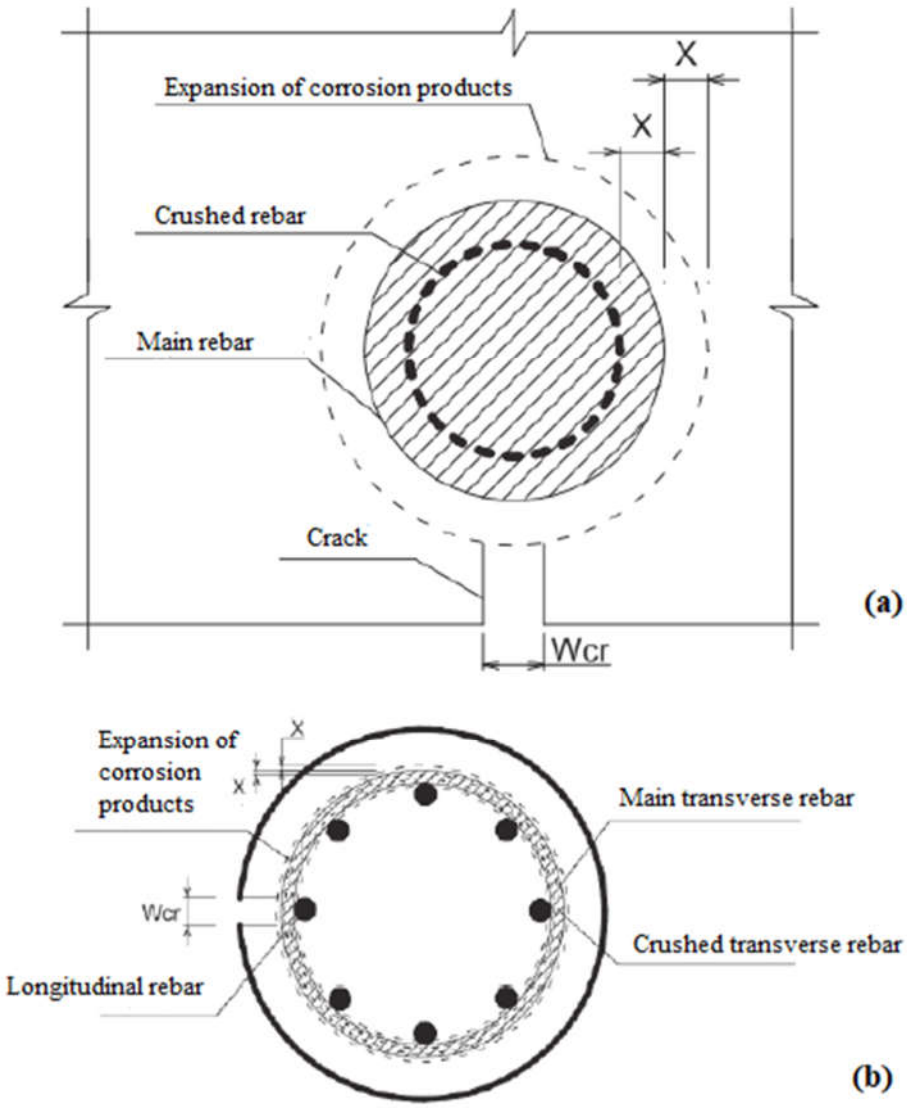

Figure 1. Crack width of corroded cover concrete (a) longitudinal rebar (b) transverse rebar.

Tensile stress due to corrosion in the cover concrete is applied as a softening coefficient on the stress-strain curve of the cover concrete. The softening behavior of concrete is considered using the softening coefficient ζ:

$$\zeta = \frac{9}{10\sqrt{1+600\varepsilon_r}} \tag{7}$$

By applying the softening coefficient of the cover concrete due to corrosion, the ascending and descending branch of the stress-strain relationship of the cover concrete has been calculated based on the Eqs 8 and 9, respectively [24]:

$$\sigma = \zeta f_c' \left[2\left(\frac{\varepsilon}{\zeta \times \varepsilon_0}\right) - \left(\frac{\varepsilon}{\zeta \times \varepsilon_0}\right)^2\right] \tag{8}$$

$$\sigma = \zeta f_c' \left[1 - \left(\frac{\frac{\varepsilon - \zeta\varepsilon_0}{\zeta\varepsilon_0}}{\frac{2-\zeta}{\zeta}}\right)^2\right] \tag{9}$$

Where:
σ: Concrete compressive stress
ε: Concrete compressive strain

Preprints (www.preprints.org) | NOT PEER-REVIEWED | "Posted: 28 October 2022" doi:10.20944/preprints202210.0438.v1

f'_c: Compressive strength characteristic of concrete
ε_0: Strain corresponding to maximum stress (0.002)

The maximum point of the stress-strain curve of the cover concrete is limited to ($\zeta \times \varepsilon_0$) and the strain range is from zero to $2\varepsilon_0$.

2.3. The Effect of Corrosion on the Mechanical Properties of Steel Bar

The effect of corrosion on the steel bar is observed in the form of reduced cross-section and changed parameters of the stress-strain equation of steel. Corrosion decreases the strength and ductility of steel. Reduction yield stress (σ_y), ultimate stress (σ_u), elasticity modulus (E_s) and ultimate strain (ε_u) of corroded steel bar are mentioned in the Eq. 10 -13, respectively [6]. Index $\underline{0}$ corresponds to the initial state without corrosion effect.

$$\sigma_y = [1 - (1.98\Delta Corr)]\sigma_{y0} \quad (10)$$

$$\sigma_u = [1 - (1.57\Delta Corr)]\sigma_{u0} \quad (11)$$

$$E_s = [1 - (1.15\Delta Corr)]E_{s0} \quad (12)$$

$$\varepsilon_u = [1 - (2.59\Delta Corr)]\varepsilon_{u0} \quad (13)$$

The above equations are used to change the properties of longitudinal and transverse bars. The following symmetric stress-strain equation has been used to model the behavior of steel [31]:

$$\sigma = \sigma_y \left[\frac{\sigma_u}{\sigma_y} - \left(\frac{\sigma_u - \sigma_y}{\sigma_y}\right) \times \left(\frac{\varepsilon_u - \varepsilon}{\varepsilon_u - \varepsilon_{sh}}\right)^2\right] \quad (14)$$

Where:
σ: Steel stress
ε_{sh}: Strain hardening of steel

2.4. Effect of Corrosion on the Properties of Confined Concrete (Core)

The confined concrete model has been used to analyze the behavior of pressurized core concrete [32]. In general, the confinement coefficient of resistance (K) and the final strain of confined concrete (ε_{cu}) have been reduced due to corrosion:

$$\varepsilon_{cu} = 0.004 + \frac{1.4\rho_s f_{yh}\varepsilon_{su}}{f'_{cc}} \quad (15)$$

Where:
ρ_s: Volume ratio of the transverse bar
f_{yh}: yield resistance of the transverse bar
ε_{su}: Maximum strain of transverse bar
f'_{cc}: Compressive strength of confined concrete

The compressive strength of confined concrete is calculated using Eqs. 16 and 17:

$$f'_{cc} = Kf'_c \quad (16)$$

$$K = 2.254\sqrt{1 + \frac{7.94f'_1}{f'_c}} - \frac{f'_1}{f'_c} - 1.254 \quad (17)$$

The effective confinement stress (f'_1) is determined using Eqs. 18 to 20:

$$f'_1 = 0.5K_e\rho_s f_{yh} \quad (18)$$

Preprints (www.preprints.org) | NOT PEER-REVIEWED | "Posted: 28 October 2022" doi:10.20944/preprints202210.0438.v1

$$K_e = \frac{(1 - \frac{s'}{2d_s})^2}{1 - \rho_{cc}} \quad (19)$$

$$\rho_s = \frac{(4A_{sp})^2}{d_s S} \quad (20)$$

Where:
K_e: Confinement effect coefficient
d_s: The diameter of the core concrete
ρ_{cc}: The ratio of the cross-section of the longitudinal steel bar to the core
s: Vertical distance of transverse bars
s': Net vertical distance of transverse bars
A_{sp}: Cross-section of transverse bars

The effect of corrosion on the properties of core concrete is reflected by the reduced cross-sectional area of the steel bar in the calculation of the cross-sectional ratio of the longitudinal bar to the core concrete (ρ_{cc}) and the volume ratio of the transverse bar (ρ_s) to confinement coefficient (K). Also, the maximum strain of concrete (ε_{cu}) is decreased by reducing the maximum strain of steel (ε_{su}). The properties of longitudinal and transverse bars have also been changed according to Eqs. 10 -13.

The stress-strain relationship in confined concrete is determined using Eq. 21:

$$\sigma = \frac{f'_{cc} \times x_c \times r}{r - 1 + x^r} \quad (21)$$

Where:

x_c: The ratio of the desired strain to the corresponding strain of the maximum compressive stress of the confined concrete

r: The ratio of the elastic modulus (E_s) to the difference between the elastic modulus and the secant modulus of confined concrete (E_{sec}) value. The relationships of these parameters are listed in Eqs. 22 -25:

$$E_c = 5000\sqrt{f'_c} \quad (22)$$

$$E_{sec} = \frac{f'_{cc}}{\varepsilon_{cc}} \quad (23)$$

$$x_\varepsilon = \frac{\varepsilon}{\varepsilon_{cc}} \quad (24)$$

$$\varepsilon_{cc} = \varepsilon_{co}\left[1 + 5(\frac{f'_{cc}}{f'_c} - 1)\right] \quad (25)$$

Where:
σ: Compressive stress of concrete
ε: Compressive strain of concrete
ε_{cc}: The strain corresponding to the maximum stress of the confined concrete
ε_{co}: Strain corresponding to the maximum stress of the initial concrete (0.002)

As mentioned before, the maximum compressive stress (strength) and final strain (ductility) is reduced in the stress-strain diagram of confined concrete due to corrosion.

2.5. Effect of Corrosion on the Connection between Concrete and Steel Bar

One of the effects of corrosion on RC materials is the progressive deterioration of the bonding between concrete and steel, which occurred as a function of corrosion level. Mechanisms of reducing the cross-sectional area of steel bar and cracking that happen due to volumetric expansion of corrosion products lead to weakened bonding. The concept of

Preprints (www.preprints.org) | NOT PEER-REVIEWED | "Posted: 28 October 2022" doi:10.20944/preprints202210.0438.v1

equivalent discontinuity length [20] has been used to investigate the corrosion effects on the reduction of this bonding. In this sense, decrement of bonding strength is showed by applying a coefficient to the stress-strain curve of the steel. Decreased continuity delays the development of stress proportionate to the increase in strain. Therefore, in exchange for the existing strain, the stress in the steel is reduced due to the joint deterioration.

Bonding reduction coefficient is defined as follows:

$$\psi = \frac{L_{eu1}}{L_{eu2}} \tag{26}$$

Where:
Ψ: Coefficient related to corrosion-induced connection reduction
L_{eu1}: Equivalent discontinuity length of the main steel bar
L_{eu2}: Equivalent discontinuity length of corroded steel bar

Assuming a uniform strain distribution, the equivalent discontinuity length is determined using the following equation:

$$L_{eu} = \frac{S_E}{\varepsilon_s} \tag{27}$$

Where:
S_E: Bar slip
ε_s: Maximum strain of bar

If the maximum available strain of the bar (ε_s) is less than the flow strain of the bar (ε_y), bar slip is calculated using Eq. 28, otherwise using Eq. 29:

$$S_E = \varepsilon_s \frac{L_{d1}}{2} \tag{28}$$

$$S_E = \varepsilon_y \frac{L_{d1}}{2} + (\varepsilon_s + \varepsilon_y) \frac{L_{d2}}{2} \tag{29}$$

In the above equations, if the existing bar stress is less than its yield stress (f_y), L_{d1} is the connection length required to transfer the bar force corresponding to the maximum available bar stress (f_s). If the maximum available stress of the bar is greater than its yield stress, L_{d2} is the required connection length to transfer the force difference between the existing force of the bar and its yield force:

$$L_{d1} = \frac{f_s d_b}{4\tau_{max}} \ , \qquad L_{d2} = \frac{(f_s - f_y) d_b}{4\tau_f} \tag{30}$$

Where:
τ_{max}: Maximum continuity resistance
τ_f: Residual bonding resistance

The maximum and residual bonding resistances are calculated using Eq. 31:

$$\tau_{max} = \sqrt{f_c'}\ (MPa) \ , \qquad \tau_f = 0.15\tau_{max} \tag{31}$$

The effect of corrosion on the bonding between concrete and steel is modeled as reducing the maximum bonding strength. The effect of corrosion on the bonding between concrete and steel is modeled as reducing the maximum bonding strength. The relationship between maximum resistance in the initial state without corrosion (τ_{max0}) and corroded state (τ_{max}) is as follows [7]:

$$\tau_{max} = (1 - D_c)\tau_{max0} \tag{32}$$

Where:
D_c: Coefficient of the maximum continuity resistance reduction

Preprints (www.preprints.org) | NOT PEER-REVIEWED | "Posted: 28 October 2022" doi:10.20944/preprints202210.0438.v1

The coefficient of the maximum bonding strength reduction is zero if the reduction of the steel's cross-sectional area due to corrosion (ΔA_s) is less than the reduction of the steel's cross-sectional area which is required to start cracking (ΔA_{s0}):

$$D_c = 1 - \left(\frac{A_s - \Delta A_s}{A_s - \Delta A_{s0}}\right)^5 \quad (33)$$

Where, A_s: The cross-section of the steel before corrosion
the cross-sectional area of the steel required to start cracking (ΔA_{s0}) is determined using Eq. 34:

$$\Delta A_0 = A_s \left[1 - \left[1 - \frac{\alpha}{d_b}(0.00753 + 0.00932\frac{d_c}{d_b}\right]^2\right] \quad (34)$$

Where:
α: Corrosion penetration depth coefficient (α = 6)
d_b and d_c: Diameter and thickness of steel bar cover, respectively

3. Modeling of the Reinforced Concrete Bridge under Study

In this section, the RCB in Iran's southern regions (with corrosive environmental conditions) has been modeled in SAP2000 software [33] to study the effect of corrosion on the long-term seismic performance of the studied bridge.

The studied bridge is a standard four-span bridge with three-pillar foundations. The deck is constructed with precast concrete beams and in-situ slabs. The bridge has two side spans, a 24 meter and a 20-meter middle span with a total length of 92 meters. The deck is discontinuous at the base, and the beams are located at the base on elastomeric supports. The general specifications of the bridge are presented in Table 1, and its model is shown in Fig. 2.

Table 1. General characteristics of bridge

Parameter	Value
Total width of deck	11.3m
Depth of deck	1.4m
Specifications of deck's transverse cross-section	A=5.196m^2 ; J= 0.1208m^4 I_x= 1.0675m^4; I_y= 59.157m^4 A_{vx}= 2.472m^2 ; A_{vy}= 2.632m^3 S_x= 2.115m^3 ; S_y= 10.4702m^3 Z_x= 2.004m^3 ; Z_y= 15.2292m^3
Height of column	6.1m
Diameter of column	1.2m
Dimensions of column capital beam	1.7 × 1.2m
Compressive strength of concrete	34.34MPa (350 kg/cm^3)
Rebar flowing strength	392.4MPa (400 kg/cm^3)
Water to cement ratio of concrete	0.4
Micro silica contents of concrete	7
Longitudinal rebar of column	12 φ 32
Transverse rebar of column	φ10 @ 7.5cm
Thickness of cover	6cm

Preprints (www.preprints.org) | NOT PEER-REVIEWED | "Posted: 28 October 2022" doi:10.20944/preprints202210.0438.v1

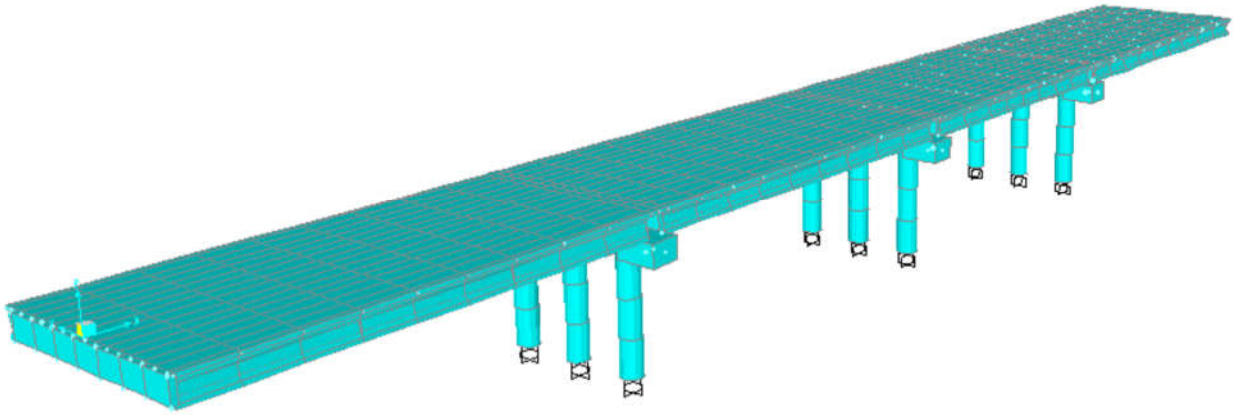

Figure 2. Model of studying RC bridge.

For seismic analysis of the bridge, three-dimensional beam-column elements with corresponding cross-sectional characteristics have been used to model the superstructure and foundation members (column and column beam). Each deck opening and the base is divided into five elements of the same length and the head beam into four elements to estimate the mass of the bridge members with the objects concentrated in the nodes,. The deck is modeled as a linear elastic beam-column element with material properties corresponding to cracking RC. No nonlinear properties are considered for the deck in overall bridge analysis. To estimate the real value for the bridge rotation period, cracking which occurred before reaching the final limit was considered and a coefficient of 0.75 was used to reduce bending moment inertia of the deck cross-section. The geometric properties of the deck are listed in Table 1. In the studied bridge with multi-column foundations, an elastic frame element with a rectangular cross-section corresponding to the dimensions of executive plans has been used to model the column capital beam. Because the superstructure concrete and the column capital beam are poured simultaneously, the flexural rigidity of the superstructure leads to a significant increase in the flexural rigidity of the column capital beam. Therefore, for realistic modeling of the column capital beam, the bending moment of the column capital beam is intensified using the coefficient of 100. It is suggested that a separate piece should be introduced at the top of the column with a specified length that represents part of the column located at the column capital beam. The specified length is equal to the distance from the top of the column to the superstructure's center of gravity. This distance is modeled as a rigid area [34]. For bridge pillars that are designed as ductile members with nonlinear behavior, effective flexural rigidity caused by cracking has been used in modeling. Assuming the axial load level is obtained from the dead load of the column, the effective flexural stiffness (I_{eff}) is defined using the following equation:

$$I_{eff} = \frac{M_Y}{E\phi_Y} \tag{35}$$

Where:
M_Y: Effective yield moment
ϕ_Y: Effective curvature
E: Elastic modulus of concrete

The effective yield moment and curvature are determined by bi-linearizing the moment-curvature curve obtained from the column cross-section analysis. Flexural and shear stiffness of concrete members are mainly reduced after the beginning of cracking. So coefficient 0.2 has been used to reduce the torsional moment of inertia, and coefficient 0.8 has been used to reduce the column's shear cross-section. According to the characteristics of the used elastomeric abutment, the longitudinal and vertical stiffness of this abutment are 3270kN/m and 62550kN/m, respectively. Since shear switch comes along the

 doi:10.20944/preprints202210.0438.v1

transverse movement of the beams (in center abutment), infinite stiffness has been used to model transverse stiffness of the abutment. The abutment of pillars' base modeled as clamped. In addition to calculating the weight of the bridge members, the dead load of the deck's asphalt superstructure, concrete fence and sidewalk of the bridge is considered 2.6kN/m^2 in the loading of the bridge.

Abutment model of the bridge consists of a rigid element with a length equal to the deck's width that is connected to the centerline of the deck through a rigid point. It has a nonlinear longitudinal, transverse and vertical response defined at each end of this rigid element [34]. The series system in the longitudinal direction are defined that consists of a rigid element with a terminal boundary condition that only allows longitudinal transmission and a length-zero element. Elastoplastic endurance curve with abutment hardness equal to 15.98kN/mm and ultimate strength of the abutment equal to 1111.1kN is allocated to the element with length-zero. If longitudinal displacement in the deck is greater than the gap between the deck and the abutment (equal to 50mm) the behavior determined for the longitudinal response will be activated. In the transverse direction, the length-zero element at each end of the rigid element is defined by elastoplastic endurance curve with a hardness of 19.78kN/mm and a final strength of 461.3 kN. In order to calculate abutment stiffness of the transverse bar, the values of the longitudinal direction have been corrected using coefficient corresponding to the effective wall length (equal to 4.3) and the participation coefficient (equal to 2.3). Length of the return wall is one-third of the back wall length. In the vertical direction, an elastic spring at each end of the rigid element is considered with a stiffness corresponding to vertical stiffness of the elastomeric abutment.

4. Overloading Analysis of the Studied Bridge

In order to seismically evaluate the studied bridge under the effect of corrosion, overloading analysis (nonlinear static) has been used. The corroded column capacity model is used for validation based on laboratory results [29]. The main purpose of this study is to compare capacity curves of the studied bridge at different times selected in its useful life. With this comparison, the effect of corrosion on the RCB capacity at any point in time can be determined. The time-zero indicates the intact bridge without corrosion. In each of other selected times, effects of corrosion on the characteristics of RC column of the bridge, including deterioration of the core concrete properties, cover concrete, steel bar and the bonding between concrete and steel bar are considered in accordance with Section 2. In the overloading analysis, properties of the plastic hinge assigned to the structure, reflect the nonlinear behavior of the structure; therefore, plastic hinges of the bridge, which are formed under seismic loading- mainly in the bridge piers- will determine the capacity curve of the bridge. The plastic hinge is usually formed at both ends of the column. To evaluate the seismic performance of the bridge under corrosion, the assumption of corrosion development in plastic hinge formation areas is reasonable and will be the basis for this study. So, at selected time-points, properties of the plastic hinge after corrosion must be updated. The overloading analysis procedure considering corrosion is done to develop the bridge capacity curve (Fig. 3).

 doi:10.20944/preprints202210.0438.v1

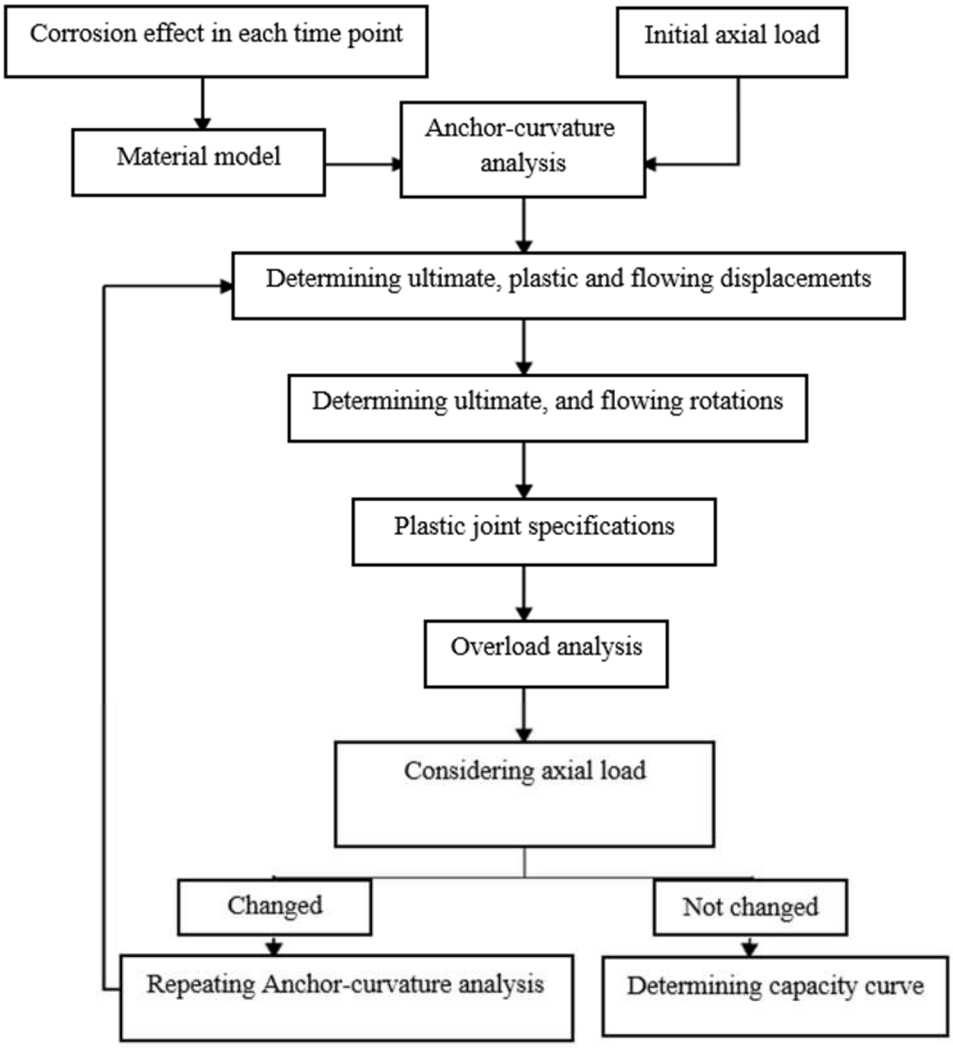

Figure 3. Pushover analysis procedure of bridge.

As it is shown in Fig. 3, the first step is to determine the material model at each time-point with corrosion. The material model includes the stress-strain behavior of the modified concrete and steel in accordance with the description in Section 2. According to the initial axial load, and the developed material model, the moment-curvature analysis of the bridge column-section was performed at any time-point and plastic hinge properties were adjusted based on the results of this analysis. Finally, overloading analysis of the bridge has been performed to determine the capacity curve of the bridge in each of selected time-points.

The plastic hinge of the column can be modeled as a centralized plasticity model in SAP2000 software using a non-coupled joint in the bending direction of M_2 and M_3 corresponding to the local axis 2-2 and 3-3 (transverse and longitudinal directions of the bridge, respectively).

The bridge studied in this research has a single column, and cantilever function in the longitudinal direction and plastic hinge formation probably will be at the longitudinal direction in the column foot. In the transverse direction, the bridge has a frame function, and due to the double curvature that occurs in the column in the transverse direction, a plastic hinge will probably form at both ends of the column. Therefore, corresponding to the longitudinal direction of the bridge, the plastic hinge M_3 is defined at the column foot and corresponding to the transverse direction of the plastic hinge M_2 it is defined at both column's ends. The length of the plastic hinge is calculated according to Eq. 36 [35]:

Preprints (www.preprints.org) | NOT PEER-REVIEWED | "Posted: 28 October 2022" doi:10.20944/preprints202210.0438.v1

$$L_p = 0.08H + 0.022f_{ye}d_{bl} \geq 0.044f_{ye}d_{bl} \quad (36)$$

Where:
L_p: Plastic hinge length (mm)
H: Column height (mm)
f_{ye}: yield strength of longitudinal bars (MPa)
d_{bl}: diameter of longitudinal bars (MPa)

The axial dead load of the column includes the branch weight of the superstructure and weight of the members themselves. Considering cantilever function of the bridge in the longitudinal direction, changes in the axial load of the column do not occur during overloading analysis; While in the transverse direction, due to the frame performance of the bridge, changes in axial load of the column occur during overloading analysis and axial load of the column at the end of overloading curve of the bridge will not be equal to the initial axial load of the column. Therefore, the axial load changes should be considered to determine the capacity curve for the transverse direction of the bridge (Fig.3).

In this research, XTRACT software has been used to perform moment-curvature analysis [36]. In order to determine properties of the plastic hinge, curvature and yield values corresponding to the yield moment (ϕ_Y, M_y), effective yield moment (ϕ_Y, M_Y) and final capacity (ϕ_p, M_P) are calculated based on the moment-curvature analysis of the column under initial axial load which is due to the dead load of the bridge. The values of effective yield moment are determined using the concept of bi-*linearization* of *Moment-Curvature Curve.* The elastic period of the structure does not change with the definition and assignment of the unpaired joint. The nonlinear behavior of the plastic hinge is defined by the normalized moment–rotation (M-θ) equation related to the effective yield moment (Fig.4). Therefore, curvature values obtained from the column moment-curvature analysis must be converted to the rotation value. Point A corresponds to the point-zero, point B corresponds to the effective yield moment (M_Y-θ_Y) and point C corresponds to the ultimate capacity point are to prevent overtaking plastic capacity of the column and bridge pier shear as a plastic hinge (M_P-θ_P). Point D corresponds to the decay point, is equivalent to 20% of the plastic capacity of the column and point E is defined as the breaking point of the column.

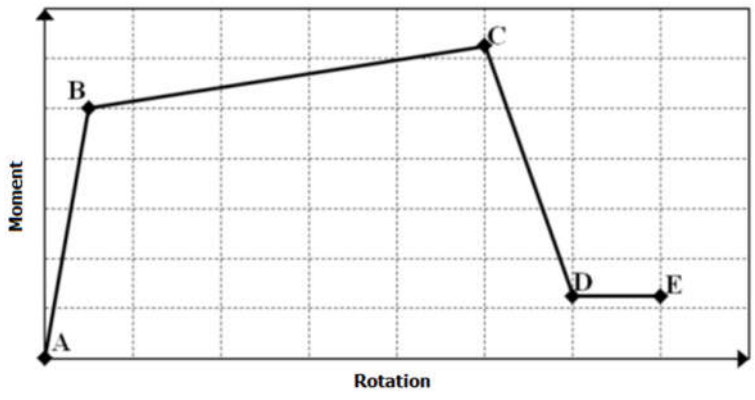

Figure 4. Defined nonlinear behavior for plastic hinge.

In order to convert the curvature values obtained from the moment-curvature analysis to displacement values and in the next step, to the column rotation values, the Eqs. 37 to 39 have been used. In these equations, plastic curvature is assumed to be constant along the plastic hinge.

$$\theta_p = (\phi_u - \phi_Y)L_p \quad (37)$$

Preprints (www.preprints.org) | NOT PEER-REVIEWED | "Posted: 28 October 2022" doi:10.20944/preprints202210.0438.v1

$$\Delta_y = \frac{H^2 \phi_Y}{3} \quad (38)$$

$$\Delta_p = \theta_p (H - \frac{L_p}{2}) \quad (39)$$

Where:
θ_P: column plastic rotation
ϕ_u: The final curvature of the column
ϕ_Y: Effective yield curvature (nominal curvature) of the column
L_P: Plastic hinge length
Δ_y: Yield displacement of the column
H: Column height
Δ_P: Plastic displacement of the column

5. Results

In the concrete mixture design of the bridge piers, water to cement ratio is 0.4 and micro-silica is 7% (Table 1). Based on our calculation and reference [28], coefficient B_1 and C_1 are 23.845 and 2.808, respectively. Since the cover thickness of the transverse bar (60 mm) and longitudinal bar (70 mm) are fixed, using Eq. 2, gives the beginning time of corrosion for the longitudinal and transverse bar which are 15.4 and 10 years, respectively. The reduced diameters of corroded longitudinal and transverse bars are calculated based on Eq. 3 and their values at the desired time-points are listed in Table 2. The longitudinal and transverse bars corrosion level is calculated based on Eq. 4 and the corrosion-time diagram is shown in Fig. 5. Since transverse bar cover is thinner than a longitudinal bar, the transverse bar corrosion starts faster, and its corrosion level is higher.

Table 2. Reduced diameter of corroded longitudinal and transverse reinforcements.

Time (year)	Longitudinal rebar's diameter (mm)	Transverse rebar's diameter (mm)
0	32	10
15	32	9.87
30	31.77	9.66
45	31.62	9.49
60	31.49	9.35
75	31.36	9.22
90	31.26	9.09

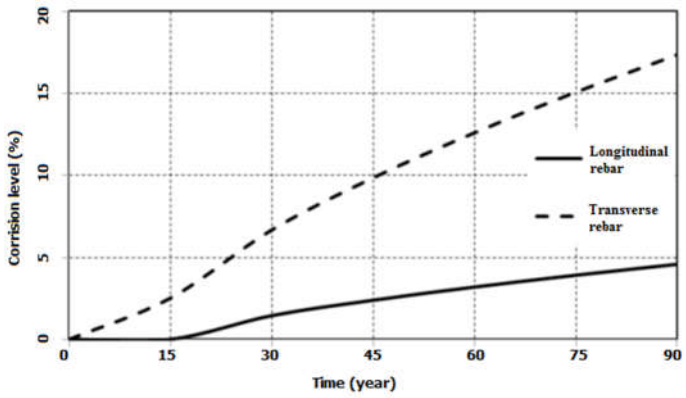

Figure 5. Corrosion level of longitudinal and transverse reinforcements.

The effect of corrosion on the unconfined concrete (cover) properties is calculated based on the equations in Section 2.2. The strain corresponding to the maximum stress and the maximum stress of the cover concrete at the desired time-points are listed in Table

 doi:10.20944/preprints202210.0438.v1

3. The stress-strain curve of the cover concrete is shown in Fig. 6. The results show a 66% reduction in maximum stress due to corrosion.

Only results for time-points 0, 30, 60 and 90 years are presented for better identification. Point zero indicates the intact state without the effect of corrosion.

Table 3. Corrosion effect on the cover concrete characteristics.

Time (year)	Strain corresponded to maximum stress	Maximum stress (MPa)
0	0.002	34.34
15	0.0018	29.95
30	0.001	17.11
45	0.0009	14.23
60	0.0008	12.66
75	0.0007	10.84
90	0.0006	11.61

The corrosion effect on the steel bar properties is calculated according to Section 2-3, and the effect of corroded concrete and steel bar on the bar behavior is calculated according to Section 2-4. The effect of corrosion on the yield and ultimate stress of steel shows a decrease of 9% and 7% at time-point of 90 years compared to the state without corrosion equivalent to the time-point zero.

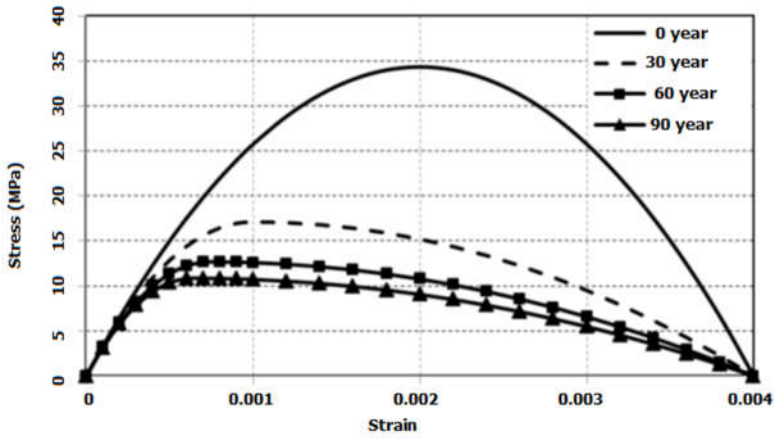

Figure 6. Stress-strain diagram of corroded cover concrete.

The corrosion effect on steel strain, with/without considering the deterioration of the bonding between concrete and steel bar, is listed in Table 4. Decreased continuity delays the development of stress in proportion to the increase in strain. Therefore, considering hinge deterioration, the bar will reach the same level of stress at the highest strain as in the initial state. A comparison between the stress-strain diagrams of the bar at time zero and 90, with /without considering corrosion loss, is shown in Fig. 7. The stress-strain diagram of steel with corrosion at the desired time-points with respect to the hinge deterioration is presented in Fig. 8. The ultimate strain of steel with corrosion has been reduced by 12%. Considering the hinge deterioration, the ultimate strain of corroded bar during 90 years has increased by 18%.

Preprints (www.preprints.org) | NOT PEER-REVIEWED | "Posted: 28 October 2022" doi:10.20944/preprints202210.0438.v1

Table 4. Corrosion effect on the steel ultimate strain.

Time (year)	Ultimate strain without considering continues detrition	Ultimate strain without considering continues detrition
0	0.2	0.2
15	0.2	0.2
30	0.1925	0.1962
45	0.1876	0.2006
60	0.1835	0.2044
75	0.1798	0.2079
90	0.1762	0.2072

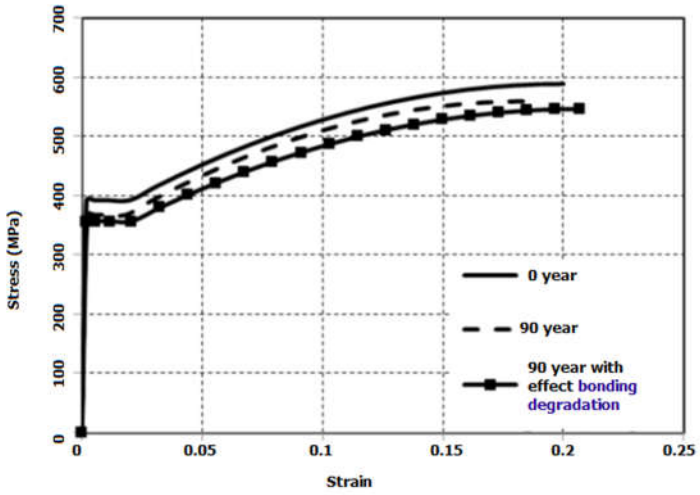

Figure 7. Effect of corrosion-induced bonding degradation on the behavior of steel.

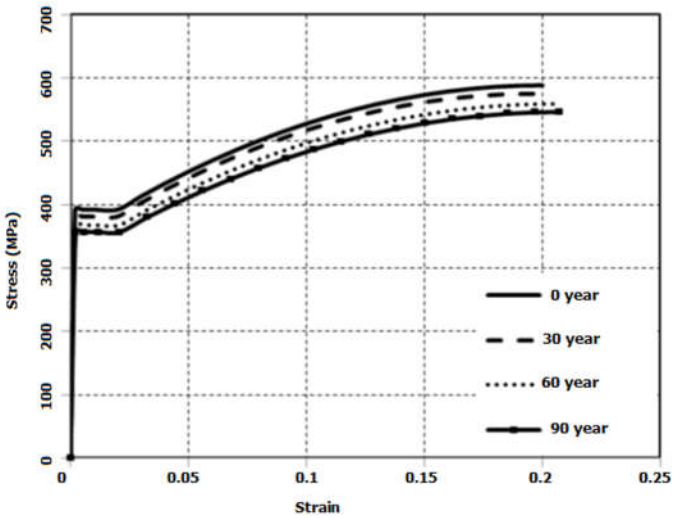

Figure 8. Stress-strain diagram of corroded steel considering the bonding degradation between concrete and steel.

The effect of corrosion on properties of confined concrete (core) is calculated according to the equations in Section 2-4. The ultimate strain and maximum stress of core concrete at different time-points are listed in Table 5, and the stress-strain curve of the core concrete is shown in Fig. 9. The strength and ductility of corroded core concrete is reduced. The maximum stress and ultimate strain of the core concrete showed a decrease of 3% and 39%, respectively.

Preprints (www.preprints.org) | NOT PEER-REVIEWED | "Posted: 28 October 2022" doi:10.20944/preprints202210.0438.v1

Table 5. Corrosion effect on the core concrete characteristics.

Time (year)	Ultimate strain	Maximum stress (MPa)
0	0.0147	40.05
15	0.0138	39.92
30	0.0124	39.72
45	0.0113	39.55
60	0.0105	39.41
75	0.0097	39.27
90	0.009	39.14

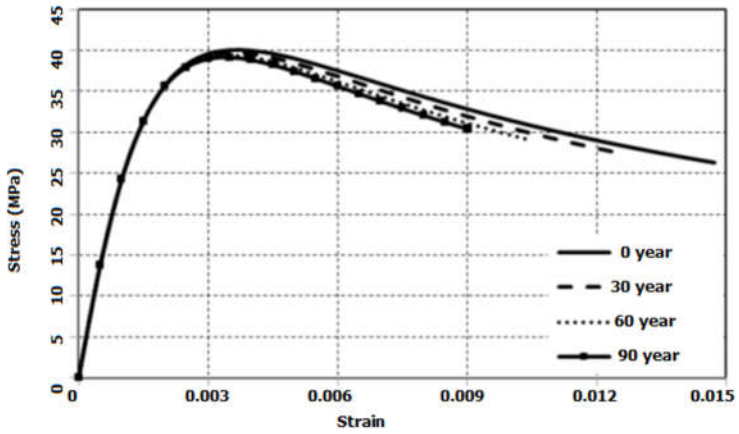

Figure 9. Stress-strain diagram of corroded core concrete.

Based on the stress-strain behavior obtained for cover concrete, core concrete and steel bar, the moment-curvature analysis of the bridge column is performed by considering the initial axial load due to the dead load of the bridge. The moment-curvature diagram related to the cross-section of the selected RC column at desired time points is shown in Fig. 10. The results show a decrease in strength and ductility. Moreover, related results to the effective yield and ultimate moment at the desired time-points are listed in Table 6. At the time point 90 years, the effective yield and ultimate moment decreased by 12% and 11%, respectively. Also, the effective and ultimate curvature yield decreased by 20% and 37%, respectively. The energy per unit length of the column, as the area below the moment-curvature diagram, decreased 43%, the plastic rotation capacity, according to Eq. 37 showed a 38% decrease. The curvature ductility, as a result of dividing ultimate curvature by the effective yield curvature, showed a reduction of 24%.

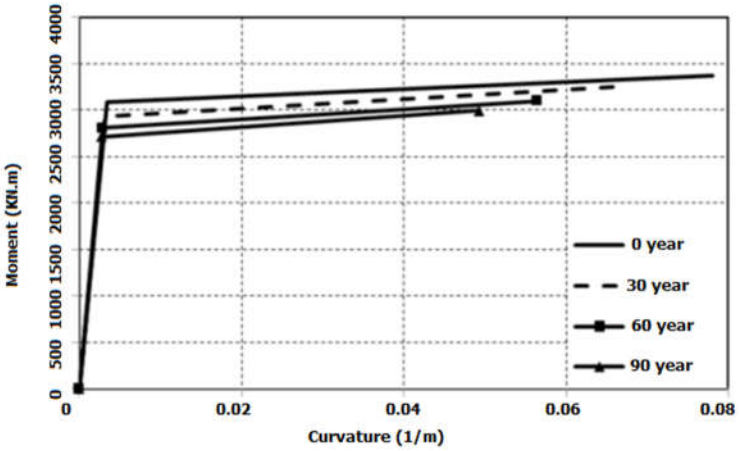

Figure 10. Moment-curvature diagram of corroded RC column.

Preprints (www.preprints.org) | NOT PEER-REVIEWED | "Posted: 28 October 2022" doi:10.20944/preprints202210.0438.v1

Table 6. Effective yield and ultimate moments of corroded section.

Time (year)	Effective flowing anchored (kN.m)	Ultimate anchored (kN.m)
0	3086	3366
15	3072	3341
30	2935	3243
45	2867	3166
60	2808	3098
75	2752	3039
90	2711	2994

Graphs of energy reduction per unit length, plastic rotation capacity and column curvature ductility over time are shown in Fig. 11, 12 and 13, respectively.

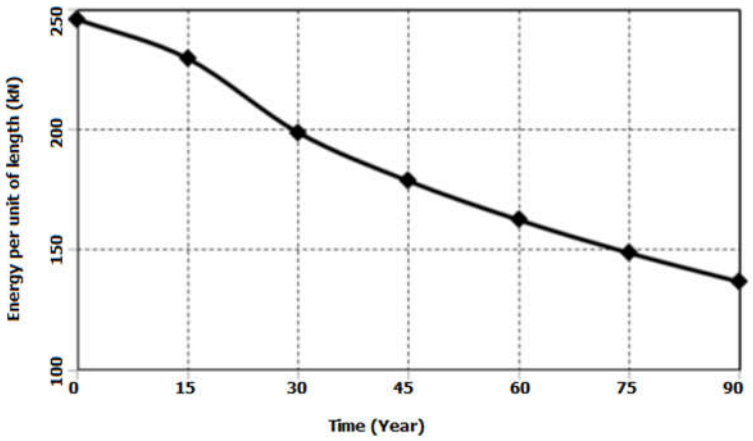

Figure 11. Reduction of energy per length of corroded column.

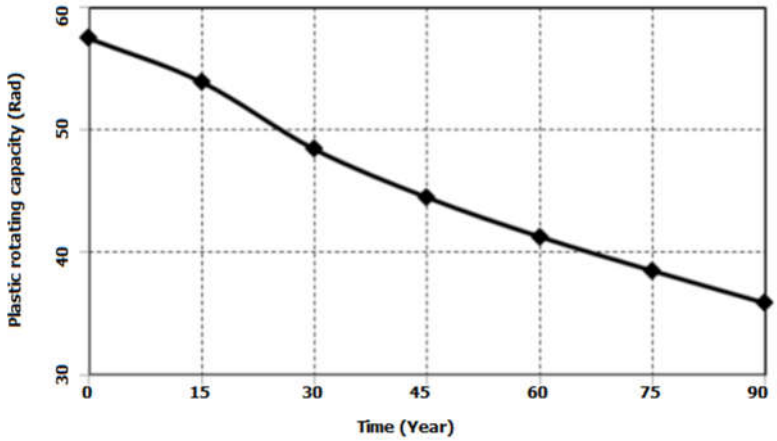

Figure 12. Reduction of plastic rotation capacity (*10^{-3}) of corroded column.

Preprints (www.preprints.org) | NOT PEER-REVIEWED | "Posted: 28 October 2022" doi:10.20944/preprints202210.0438.v1

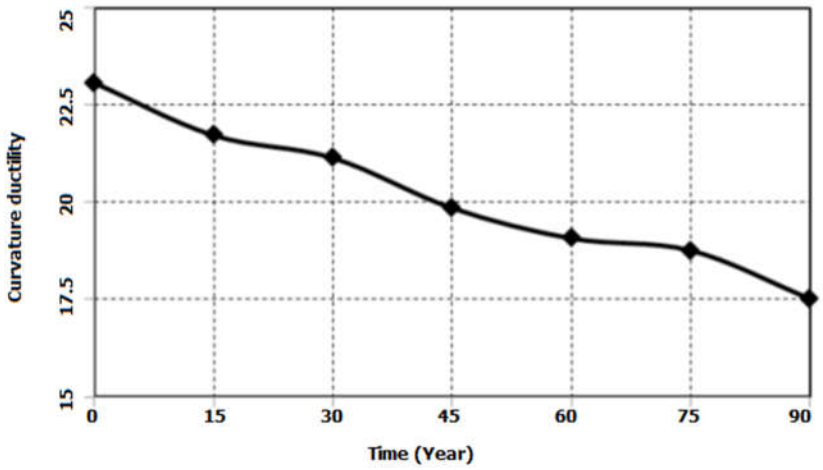

Figure 13. Reduction of curvature ductility of corroded column.

According to the results of moment-curvature analysis and their conversion to moment-rotation values based on relations 37 to 39, the characteristics of plastic hinges at each time point are adjusted. Overloading analysis of the bridge in both longitudinal and transverse directions is shown in Fig. 3. The results of the maximum base shear and the corresponding displacement for the longitudinal and transverse directions of the bridge are presented in Table 7 and Table 8, respectively. The capacity curve (overloading curve) of the bridge in both longitudinal and transverse directions is shown in Fig. 14 and 15, respectively.

In the longitudinal and transverse directions of the bridge at the time-point of 90 years, the maximum base shear reduced by 11.5% and 12.5%, respectively. Therefore, to ensure the seismic performance of the bridge under 90-year corrosion, the base shear design can be increased by 12.5%. At each of other time-points, the amount of increase in the base shear design can be determined by similar calculations.

Table 7. Maximum base shear and corresponding displacement in the longitudinal pushover analysis of bridge.

Time (year)	Maximum displacement (mm)	Maximum shear (kN)
0	413.92	1471.04
15	390.57	1462.13
30	349.45	1403.76
45	323.79	1375.1
60	30.09	1346.41
75	281.41	1319.64
90	265.75	1300.69

Table 8. Maximum base shear and corresponding displacement in the transverse pushover analysis of bridge.

Time (year)	Maximum displacement (mm)	Maximum shear (kN)
0	305.03	3922.43
15	295.31	3887.97
30	206.39	3796.93
45	195.68	3708.85
60	185.62	3622.27
75	175.14	3543.47
90	170.61	3431.56

Preprints (www.preprints.org) | NOT PEER-REVIEWED | "Posted: 28 October 2022" doi:10.20944/preprints202210.0438.v1

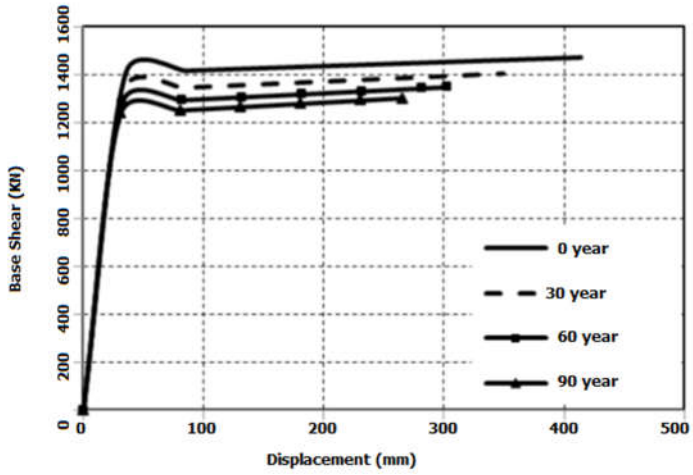

Figure 14. Longitudinal capacity curve (pushover) of bridge.

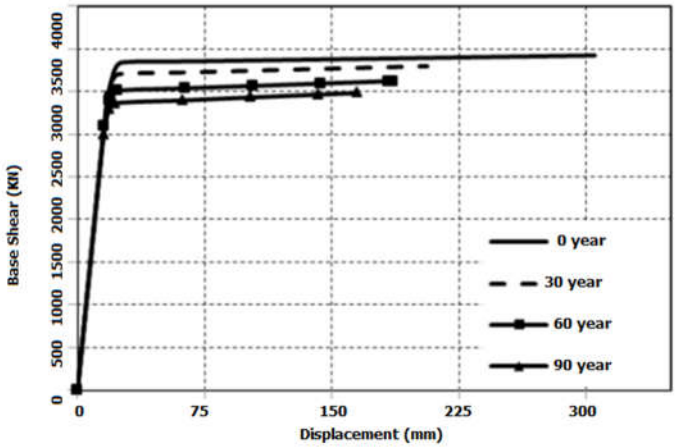

Figure 15. Transverse capacity curve (pushover) of bridge.

6. Conclusion

The present study was carried out to determine the effect of corrosion due to chloride ion diffusion on the seismic performance of RCB. In the southern regions of Iran, near the coasts of the Persian Gulf and the Sea of Oman, due to the high corrosion of RC members that is because of environmental conditions and seismicity, the seismic performance of RCB is significant. For this purpose, RCB overloading analysis in these areas under the corrosion influence has been performed, and the following results are highlighted:

Since the transverse bar cover is thinner than a longitudinal bar, corrosion starts faster in that (in 90 years). Corrosion in transverse bar cover is 3.8 times higher than a longitudinal bar.

Because of corrosion, the maximum stress of the cover concrete, yield strength of the steel and ultimate strain of the core concrete during 90 years decrease by 66%, 9% and 39%, respectively.

Moment-curvature analysis of RC columns shows a reduction of 12%, 11%, 20% and 37% of the effective yield moment, the ultimate moment and the corresponding curvature values for 90 years due to corrosion.

Energy per unit length, plastic rotation capacity and corrosive curvature ductility of the column over 90 years have decreased by 43%, 38% and 24%, respectively.

Overloading analysis of RCB shows an average reduction of 12.5% and 50%, respectively, in maximum base shear (strength criterion) and corresponding displacement (ductility criterion) due to corrosion over 90years.

Considering the results for deterioration of the bridge capacity due to corrosion, a proposal to increase the base shear design to ensure the seismic performance of RCB in corrosive environments.

To ensure the 90-year seismic performance of RCB in the southern regions of Iran (with a similar structural system of the studied bridge), the shear design can be increased by 12.5%.

Data Availability Statement: Data supporting the findings of this study are available from the corresponding author on request.

References

1. C. Q., Li, J. J., Zheng, Propagation of reinforcement corrosion in concrete and its effects on structural deterioration, Magazine of Concrete Research, 57(5) (2005) 261-71.
2. X., Shi, N., Xie, K., Fortune, J., Gong, Durability of steel reinforced concrete in chloride environments: An overview, Construction and Building Materials, 30 (2012) 125-138.
3. F. J., Molina, C., Alonso, C., Andrade, Cover cracking as a function of rebar corrosion: part 2-numerical model, Materials and structures, 26(9) (1993) 532-548.
4. D., Coronelli, P., Gambarova, Structural assessment of corroded reinforced concrete beams: modeling guidelines, Journal of Structural Engineering, 130(8) (2004) 1214-1224.
5. M. P., Enright, D. M., Frangopol, Service-life prediction of deteriorating concrete bridges, Journal of Structural engineering, 124(3) (1998) 309-317.
6. H. S., Lee, Y. S., Cho, Evaluation of the mechanical properties of steel reinforcement embedded in concrete specimen as a function of the degree of reinforcement corrosion, International journal of fracture, 157(1-2) (2009) 81-88.
7. A., Castel, I., Khan, R. I., Gilbert, Development length in reinforced concrete structures exposed to steel corrosion: A correction factor for AS3600 provisions, Australian Journal of Structural Engineering, 16(2) (2015) 89-97.
8. K., Bhargava, A. K., Ghosh, Y., Mori, S., Ramanujam, Suggested empirical models for corrosion-induced bond degradation in reinforced concrete, Journal of structural engineering, 134(2) (2008) 221-230.
9. K. A., Vu, M. G., Stewart, Structural reliability of concrete bridges including improved chloride-induced corrosion models, Structural safety, 22(4) (2000) 313-333.
10. T., Guo, R., Sause, D. M., Frangopol, A., Li, Time-dependent reliability of PSC box-girder bridge considering creep, shrinkage, and corrosion, Journal of Bridge Engineering, 16(1) (2010) 29-43.
11. C. K., Chiu, T., Noguchi, M., Kanematsu, Optimal maintenance plan for RC members by minimizing life-cycle cost including deterioration risk due to carbonation, Journal of advanced concrete technology, 6(3) (2008) 469-480.
12. E., Martinelli, E., Erduran, Seismic Capacity Design of RC frames and environment-induced degradation of materials: Any concern?, Engineering Structures, 52 (2013) 466-477.
13. L., Berto, R., Vitaliani, A., Saetta, P., Simioni, Seismic assessment of existing RC structures affected by degradation phenomena, Structural Safety, 31(4) (2009) 284-297.
14. H., Yalciner, S., Sensoy, O., Eren, Time-dependent seismic performance assessment of a single-degree-of-freedom frame subject to corrosion, Engineering Failure Analysis, 19 (2012) 109-122.
15. R., Kumar, P., Gardoni, M., Sanchez-Silva, Effect of cumulative seismic damage and corrosion on the life-cycle cost of reinforced concrete bridges, Earthquake Engineering & Structural Dynamics, 38(7) (2009) 887-905.
16. J., Zhong, Seismic fragility estimates for corroded reinforced concrete bridge structures with two-column bents, PhD Thesis, Texas A&M University, Texas, (2008).
17. J., A., Harvat, Effect of corrosion on the seismic response of a single-bent, reinforced concrete bridge". PhD Thesis, Texas A&M University, Texas, (2009).
18. J., Ghosh, J. E., Padgett, Aging considerations in the development of time-dependent seismic fragility curves, Journal of Structural Engineering, 136(12) (2010)1497-1511.
19. F., Biondini, M., Vergani, Damage modeling and nonlinear analysis of concrete bridges under corrosion, In Sixth International Conference on Bridge Maintenance, Safety and Management (IABMAS 2012), Stresa, Italy, (2012) 8-12.
20. Y. C., Ou, H. D., Fan, N. D., Nguyen, Long-term seismic performance of reinforced concrete bridges under steel reinforcement corrosion due to chloride attack, Earthquake Engineering & Structural Dynamics, 42(14) (2013) 2113-2127.
21. M., Shekarchi, F., Moradi, Concrete durability issues in the Persian Gulf, InCBM-CI International Workshop, 200 (2007) 357-370.
22. D. Li, L.Y. Li, X. Wang, Chloride diffusion model for concrete in marine environment with considering binding effect, Mar. Struct. 66 (JUL.) (2019) 44–51.
23. S. Real, J.A. Bogas, Chloride ingress into structural lightweight aggregate concrete in real marine environment, Mar. Struct. 61 (SEP.) (2018) 170–187.
24. F. Tittarelli, A. Mobili, C. Giosu`e, A. Belli, T. Bellezze, Corrosion behaviour of bare and galvanized steel in geopolymer and Ordinary Portland Cement based mortars with the same strength class exposed to chlorides, Corros. Sci. 134 (2018) 64–77.

25. H.S. Al-Alaily, A.A.A. Hassan, Time-dependence of chloride diffusion for concrete containing metakaolin, J. Build. Eng. 7 (2016) 159–169.
26. M.U. Khan, S. Ahmad, H.J. Al-Gahtani, Chloride-induced corrosion of steel in concrete: an overview on chloride diffusion and prediction of corrosion initiation time, Int J. Corros. 2017 (2017).
27. S. Muthulingam, B.N. Rao, Consistent models for estimating chloride ingress parameters in fly ash concrete, J. Build. Eng. 3 (2015) 24–38.
28. H. R., Ashrafi, A. A., Ramezanianpour, Model Presentation for the Chloride Diffusion in Silica Fume Concretes Based on the Experimental Results, PhD Thesis, Amirkabir University of Technology, Tehran, 2007.
29. D. E., Choe, P., Gardoni, D., Rosowsky, T., Haukaas, Seismic fragility estimates for reinforced concrete bridges subject to corrosion, Structural Safety, 31(4) (2009) 275-283.
30. T. T., Hsu, Unified theory of reinforced concrete, CRC press, Dec, (1992).
31. J. B., Mander, Seismic design of bridge piers, PhD Thesis, University of Canterbury, Christchurch, N.Z, (1983).
32. J. B., Mander, M. J., Priestley, R., Park, Theoretical stress-strain model for confined concrete, Journal of structural engineering, 114(8) (1988) 1804-1826.
33. CSI., SAP2000- Linear and Nonlinear Static and Dynamic Analysis and Design of Three-Dimensional Structures: Basic Analysis Reference Manual. Computers and Structures, Inc, Berekeley, California, (2005).
34. A., Aviram, K. R., Mackie, B., Stojadinović, Guidelines for nonlinear analysis of bridge structures in California. Pacific Earthquake Engineering Research Center, Berekeley, California, (2008).
35. Caltrans., Caltrans Seismic Design Criteria Version 1.6. California Department of Transportation, Sacremento, California, (2010).
36. XTRACT., Cross Section Analysis Program for Structural Engineers, IMBSEN & Associate Inc., USA, (2007).